Nanocomposites Derived from Cellulose Acetate and Highly Branched Alkoxysilane

Cristiane Aparecida da Silva, Márcia Maria Favaro, Inez Valéria Pagotto Yoshida, Maria do Carmo Gonçalves

Institute of Chemistry, University of Campinas (UNICAMP), Campinas, São Paulo, Brazil

Received 26 March 2010; accepted 13 December 2010
DOI 10.1002/app.33974
Published online 23 March 2011 in Wiley Online Library (wileyonlinelibrary.com).

ABSTRACT: Highly branched alkoxysilane (HB) units were prepared *in situ* via a Michael-type reaction between pentaerythrithol triacrylate and aminopropyltriethoxysilane. These units were used as an inorganic component for the modification of cellulose acetate (CA) films using the sol–gel process. The thermal and dynamic-mechanical behaviors, the morphology, and the dimensional stability of the modified CA films were analyzed. The siloxane-modified CA films showed thermal stability similar to pure CA, but the residue content at 900°C increased with the addition of HB units. The morphology of these films was characterized by siloxane nanodomains dispersed in the CA matrix, with good interfacial adhesion between the phases. Moreover, the CA/siloxane nanocomposite films showed improved dimensional stability in comparison with CA, i.e., in the presence of HB, the dimensional change was reduced to around 50% of the value observed for pure CA. Finally, a complex dynamic-mechanical behavior was obtained for the nanocomposite films, as a consequence of the heterogeneous morphology. © 2011 Wiley Periodicals, Inc. J Appl Polym Sci 121: 2559–2566, 2011

Key words: cellulose acetate; nanocomposites; sol–gel process; alkoxysilanes

INTRODUCTION

The major driving forces behind the intense activities in the development of organic–inorganic nanocomposites are the new and different properties that can be attained, which the traditional mixture of organic and inorganic components cannot show. Unlike traditional composite materials that have macroscale domain sizes, nanocomposites have phase domain sizes typically smaller than 100 nm.[1–6]

Organic–inorganic nanocomposites have been successfully used to prepare transparent thin films with unique physical properties.[7,8] The nature of the components and the composition of these films determine their characteristics. Usually, the inorganic phase contributes toward film stability while the organic phase, which can be a polymer, is chosen by the set of physical and chemical properties, particularly the processing characteristics. The uniformity of phase distribution is also an important parameter to define the properties of the nanocomposites.[4]

Different polymer systems have been used in hybrid nanocomposites, and biodegradable polymers from renewable resources are a fairly new area.[4,5] One good candidate for the preparation of this kind of nanocomposite is cellulose acetate (CA) owing to its potential biodegradability, excellent optical clarity, and stiffness.[9–11] This polymer is a thermoplastic produced primarily from cellulose, the most abundant natural polymer on earth and has great industrial importance as a low-cost starting material. It has applications in many areas such as support for fibers, packing films, plastic devices, filters, membranes, adhesives, coatings for paper, electrical isolation, and drug delivery systems.[12,13] However, several limitations including poor mechanical resistance, organic solvent attack, and low swelling resistance in water have limited the application of CA.[14,15] One way to overcome these limitations is the preparation of CA-based nanocomposites.

A successful route for the preparation of organic–inorganic materials is the sol–gel process. The mild reaction conditions, particularly low reaction temperatures, allow the incorporation of an inorganic component in an organic matrix, or *vice versa*. This incorporation can be done by physical dispersion or by a covalent bond between the components. By using the sol–gel process, it is possible to finely disperse an inorganic phase within an organic polymeric matrix, which sometimes reaches molecular levels. The inorganic phase can be obtained by hydrolysis followed by condensation reactions of alkoxysilane precursors, giving rise to siloxane as the inorganic dispersed phase, which can even be linked to the organic polymeric matrix. During this

Correspondence to: M. do C. Gonçalves (maria@iqm.unicamp.br).

Contract grant sponsors: FAPESP and CNPq.

process, the inorganic precursors can act as cross-linking centers in the polymeric matrix, which can increase the chemical stability or the swelling resistance of this matrix.[16–23]

Nie and Narayan[24] showed that the uniform dispersion of styrene anhydride random copolymers in a CA matrix brings new properties to the materials, such as improved dimensional stability and reduced moisture adsorption. Zoppi and Gonçalves[14] demonstrated that the incorporation of a silica phase, via the sol–gel process of hydrolysis of tetraethoxysilane (TEOS), onto a CA matrix led to more rigid films, which showed a decrease of water permeability, with thermal stability similar to pure CA. Recently, Jiang and coworkers[25] developed CA membranes with enhanced permeation and antifouling properties. These materials were prepared through the *in situ* generation of silica nanoparticles, via the hydrolysis and condensation reaction of tetraethylorthosilicate as the precursor.

The aim of this work was to prepare organic–inorganic nanocomposites, derived from CA and a highly branched alkoxysilane (HB) precursor, using the sol–gel process, and to characterize their thermal and dynamic-mechanical behaviors, their morphology and dimensional stability.

EXPERIMENTAL

Materials

CA with a number-average molar mass of 30,000 g/mol, 39.8 wt % acetyl content (degree of substitution of CA = 2.5) was purchased from Aldrich and was used as received. Commercially available pentaerythrithol triacrylate (PETA) was obtained from Dow Chemical. γ-aminopropyltrietoxysilane (APTS) and di-*n*-butyltin-dilaurate complex (Sn catalyst) were supplied by Dow Corning. Tetrahydrofuran (THF) was purchased from Merck and it was dried and distilled before use.

Sample preparation

HB cross-linker units were prepared *in situ* via a Michael-type reaction from the PETA and APTS mixture, using a stoichiometric amount of $CH{=}CH_2$ and NH_2 groups, respectively, with anhydrous THF as solvent, in a procedure similar to one previously described.[26] The synthetic procedure to prepare HB units is shown in Figure 1. First, 6.64 g (0.03 mol) of APTS and 30 mL of anhydrous THF were added to a three-necked flask equipped with a mechanical stirrer under an argon atmosphere. Next, 2.9 g (0.01 mol) PETA and 10 mL of anhydrous THF were introduced. The Michael-type reaction was carried out for 8 h at room temperature (~26°C). The resulting viscous solution was stored in a freezer.

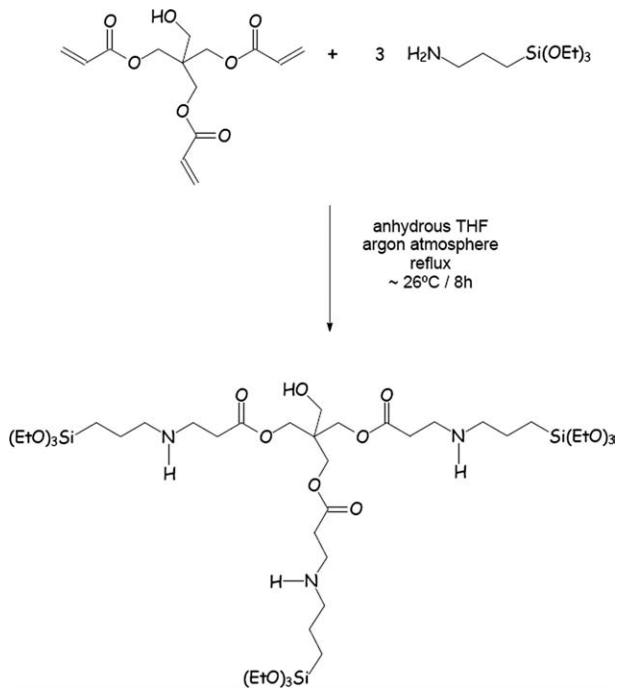

Figure 1 Proposed reaction between PETA and APTS.

Organic–inorganic cross-linked thick films derived from CA/HB precursor were prepared by the sol–gel process in the presence of a Sn^{2+} catalyst. The HB precursor was added to a three-necked flask, equipped with a mechanical stirrer and under an argon atmosphere, containing CA dissolved in anhydrous THF and Sn^{2+} catalyst (0.3 wt %). The hydrolysis and condensation reactions of the HB units were performed at 40°C for 24 h under an argon atmosphere. The viscous homogeneous solutions were cast onto Teflon™ petridishes and left to stand for 1 week, at room temperature under a water-saturated atmosphere. This procedure was carried out to promote the hydrolysis and condensation of residual reactive Si-OEt groups. The resulting HB/CA self-supported films were submitted to isothermal treatment at 70°C, in a vacuum oven, for 48 h. The HB/CA films were prepared with HB unit compositions equal to 10, 20, and 30 wt %.

Characterization

Infrared spectra were performed on a Bomem MB B100 Series spectrometer operating at 4 cm^{-1} resolution and coadding 16 scans, with the conventional KBr-supported film technique. Thermogravimetric analysis (TGA) was performed in a TA 2950 thermobalance, TA Instruments, over the 25–1000°C range, at a 20°C/min scanning rate under an argon flow. The dynamic-mechanical behaviors of pure CA and

the HB/CA films were analyzed using a DMTA V Rheometric Scientific Instrument from −50 to 250°C at 5°C/min using a fixed frequency of 1 Hz and 0.20 mm amplitude.

The morphology of the HB/CA films was examined with a JSM-6340 field emission scanning electron microscope (FESEM) from Jeol, operating at an accelerating voltage of 3.0 kV. The samples were prepared by fracturing in liquid nitrogen and mounted in the sample holder with double-sided carbon adhesive tape. The samples were carbon sputtered coated in a Bal-Tec MD 020 instrument (Balzers). The morphology of HB/CA films was also investigated by TEM using a Carl Zeiss CEM 902 transmission electron microscope (80 kV) equipped with a Castaing-Henry energy filter spectrometer within the column and a Proscan Slow Scan CCD camera. Ultrathin sections, approximately 50-nm thick, were cut perpendicular to the film plane at room temperature, ~26°C, using a diamond knife, in a Leica EM FC6 ultramicrotome. The thin sections were collected on uncoated 300 mesh copper grids (Ted Pella). Images were acquired using electrons with zero-loss energy and processed using AnalySis 3.0 software.

The free HB/CA surfaces were analyzed in a Jeol JSM-6360 LV SEM scanning electron microscope at a 20 kV accelerating voltage equipped with an energy dispersive spectrometer, EDS (NORAN System Six). The EDS analyses of the silicon content were performed on the free sample surfaces, using the standardless quantitative analysis NORAN software.

Water contact angle measurements were obtained using a Zeiss Photo-Mikroskop III optical microscope coupled to a Sony CCDIRIS video camera. The reported contact angle results, for pure CA and HB/CA films, were an average of 10 measurements at different film surface points. Deionized water was applied to obtain a 10-μL drop.

The dimensional stability of the films was evaluated according to the procedure described by Nie and Narayan.[24] The films were soaked in water at room temperature for 30 h. The dimensional changes of the films were measured after the film samples were dried naturally for 1 day. All samples had 2 × 2 cm dimensions. The changes in length were reported as a measure of dimensional stability.

RESULTS AND DISCUSSION

The alkoxysilane precursor was prepared from a stoichiometric amount of PETA and APTS by a Michael-type addition reaction. Figure 2 shows the infrared spectra of PETA, APTS, and HB units. The absorption at 1630 cm^{-1} can be assigned to C=C stretching vibration from PETA, and the peaks at 3388 cm^{-1} and 3307 cm^{-1} can be assigned to NH_2 stretching from ATPS. In the HB spectrum, a decrease in the relative intensity of absorptions from C=C and NH_2 groups was observed in addition to the relatively broad band centered at ~1030 cm^{-1}, associated to Si—OC, indicating the occurrence of the Michael-type reaction and confirming the formation of the multi-functional alkoxysilane.[27,28]

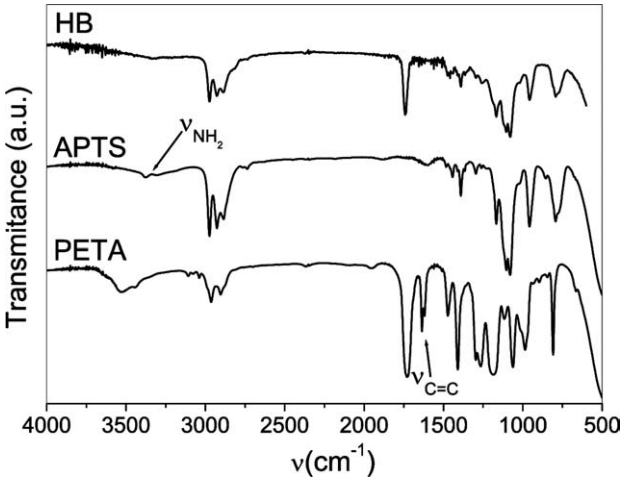

Figure 2 FTIR spectra of PETA, APTS, and HB.

Figure 3 schematically illustrates the HB/CA microstructure developed. The multifunctional alkoxysilane precursor (HB) exhibited high reactivity in relation to condensation reactions with the CH_2—OH groups of CA chains. The condensation reaction between reactive CH_2—OH (from CA chains) and Si—OEt groups (from HB precursor) could promote the cross-linking of the CA chains in the presence of Sn^{2+} catalyst, by condensation reactions.[29] Taking into account that the HB/CA films were obtained under a water-saturated atmosphere, other concomitant reactions could have occurred, such as the hydrolysis of Si-OEt from HB and self-condensation reactions involving only HB units, producing siloxane nanoclusters, rich in Si—OH groups, which could also act as cross-linker centers in the formation of the HB/CA network. José et al.[26] showed that the introduction of silica nanoclusters, obtained from TEOS as an additional cross-linker, improved the mechanical stability of hybrid organic–inorganic films based on poly(dimethylsiloxane) and also decreased the solvent sorption rate.

The thermogravimetry curves for pure CA and HB/CA films are shown in Figure 4. In the case of CA, three steps of mass loss were observed. The first step from 32 to 180°C represents the volatilization of residual water; the second step, from 180 to 300°C, is related to the loss of acetyl groups, followed by acetic acid volatilization, which catalyzed the decomposition of cellulose. The third step starts at 300°C and represents the main thermal degradation

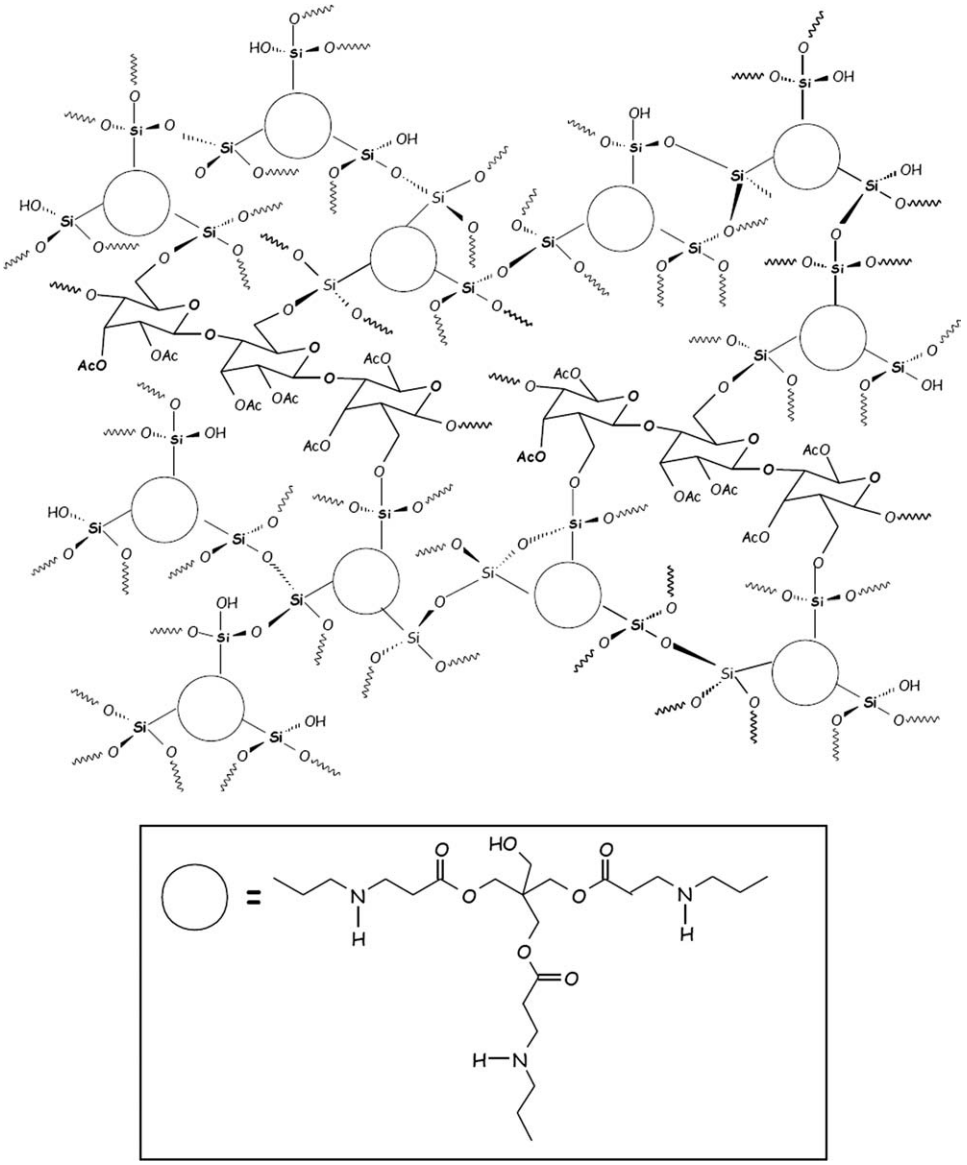

Figure 3 Synthetic concept of cellulose acetate/highly branched alkoxysilane.

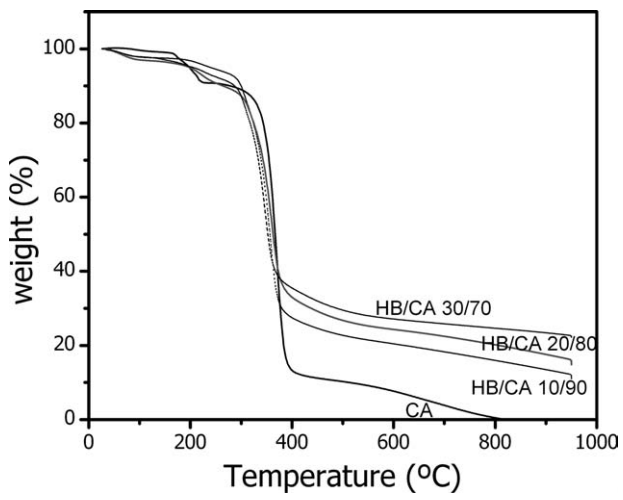

Figure 4 Thermogravimetric curves of pure CA and HB/CA films.

of cellulose chains. This degradation profile is in agreement with the Chatterjee and Conrad description for cellulosic materials.[30]

For the HB/CA films, notwithstanding the composition, the thermal stability was similar to that observed for pure CA. However, from ~175°C to ~300°C, a higher mass loss was observed due to water volatilization as a consequence of the thermal induced condensation of residual Si—OH groups. The temperatures of the maximum rate of mass loss were 368°C, 368°, 365° and 380°C for pure CA, HB/CA (10/90), HB/CA (20/80), and HB/CA (30/70), respectively. The residue percentages at 900°C were 0.0, 13.5, 17.7, and 23.4 for pure CA, HB/CA (10/90), HB/CA (20/80), and HB/CA (30/70), respectively. This increase of the residue content with the HB content suggests the successful incorporation of the polysiloxane phase in the CA.

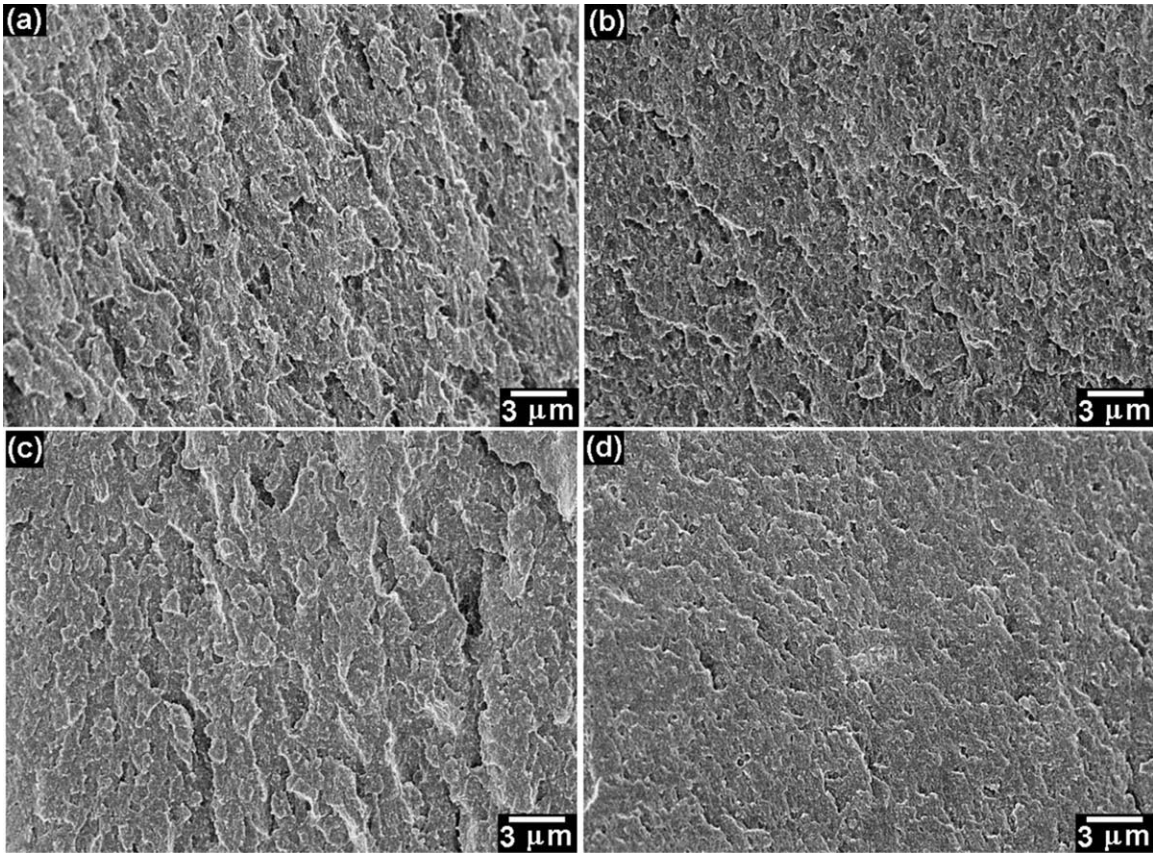

Figure 5 FESEM micrographs of bulk fractures: (a) pure CA, (b) HB/CA 10/90, (c) HB/CA 20/80, and (d) HB/CA 30/70.

The morphologies of these materials were characterized by FESEM and TEM. The HB/CA films were transparent, which indicates that if a dispersed polysiloxane phase was developed in the polymer, this phase was on a submicron scale. One of the advantages of nanocomposites is that the domain size of the dispersed phase is smaller than the wavelength of visible light so that these materials should be optically clear.

Figure 5 presents the morphological characteristics of pure CA and the HB/CA film bulk fractures investigated by FESEM. The morphology of the fractured surfaces did not show phase segregation in this analysis but only reduction of bulk roughness with the increase of HB content. On the other hand, the free surface images showed increased roughness with the increased HB content (micrographs not shown). Transmission electron micrographs of thin sections gave a new insight into their morphologies revealing domains of a second phase (Fig. 6). Dark regions in these micrographs correspond to polysiloxane nanodomains formed by the condensation of HB units. The domains showed a high polydispersion in size, ranging from a few nanometers to a hundred nanometers. These dimensions increased with increased HB content. Moreover, the TEM images showed the integrity of the interfaces between the polysiloxane nanodomains and the matrix, which indicates good interfacial adhesion, as expected from a covalent C—O—Si interface.

HB/CA films were obtained with no cracks and their chemical resistance was investigated by testing in different solvents, such as THF and acetone, which are good solvents for CA. The HB/CA films were insoluble in organic solvents, which are further evidence of the cross-linking of CA chains by condensation reactions. The films also showed good dimensional stability in water. After immersion in water for 30 h, the dimensional changes obtained were 6.0, 3.3, 3.6, and 7.1% for pure CA, HB/CA (10/90), HB/CA (20/80), and HB/CA (30/70), respectively. Thus, the dimensional change for HB/CA (10/90), and HB/CA (20/80), was reduced to around 50% of the value observed for pure CA. These results can be explained if the siloxane domains are presumed to act as an additional cross-linker in the HB/CA network. The small domain sizes and consequently the large siloxane/matrix interfacial area can reduce the free volume available for water sorption and thus contribute to the dimensional stability of the films. The negative effect for HB/CA 30/70 can be explained by the different

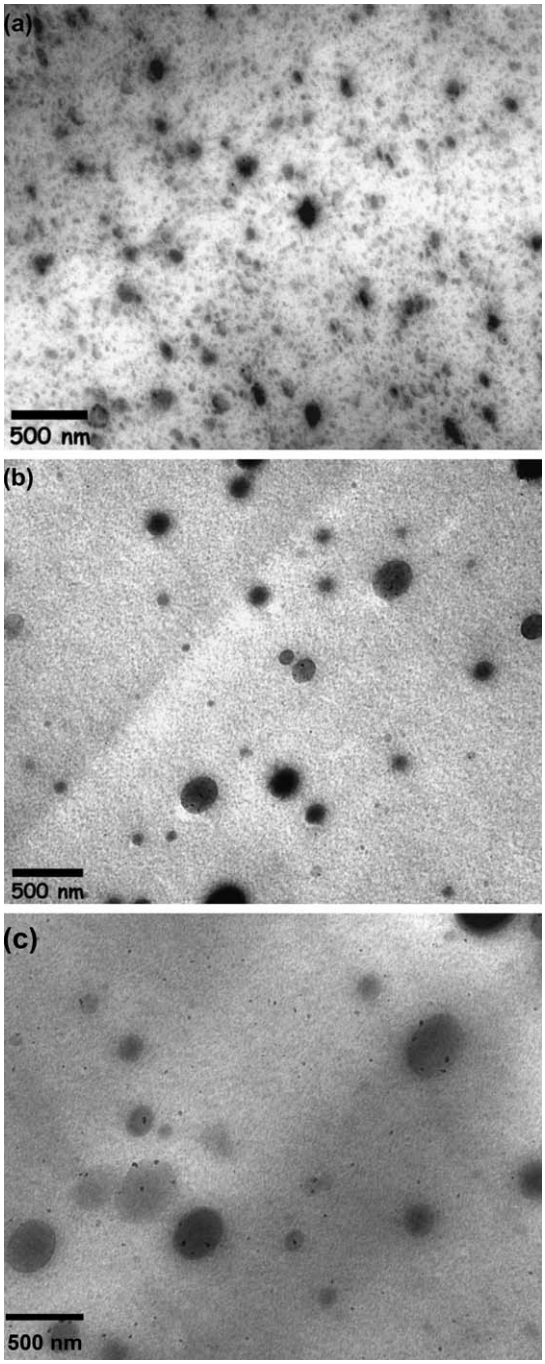

Figure 6 Transmission electron microscopy images of HB/CA nanocomposites: (a) HB/CA 10/90, (b) HB/CA 20/80, and (c) HB/CA 30/70.

morphological characteristics of this sample compared with the other nanocomposites. In the HB/CA 30/70 sample, a significant increase in the polysiloxane domain size and its poor dispersion in the matrix were observed, as illustrated in Figure 6(c).

Another characteristic of the prepared HB/CA films is the decrease of the hydrophilic character of the CA surface, as confirmed by the contact angle results presented in Table I.

TABLE I
Water Contact Angle Measurements

Sample	Average contact angle
CA	65 ± 1
HB/CA 10/90	67 ± 1
HB/CA 20/80	73 ± 2
HB/CA 30/70	84 ± 1

The surface composition of the HB/CA samples was determined by the EDS analysis of the silicon content at the free surface. Table II shows the silicon atomic content obtained experimentally from the EDS analysis and the calculated values taken from the initial compositions.

The average values of Si atomic content, obtained on the free surface of the samples, increased with the increase of the HB content. It was also observed that the calculated atomic silicon content values were always lower than the experimental values, indicating that the silicon distribution was not uniform throughout sample and that a migration to the free surface occurred. This effect can be due to the difference in the surface tensions of silanes and CA. The reported values for the former are in the range of 33.7–35.7 mN/m, whereas the value for the latter is 45.9 mN/m.[31] Thus, the lower surface tension of the functional units could explain its increase on the surface. This result corroborates the higher water contact angle values.

It is necessary to keep in mind that in the SEM-EDS analysis the element composition is obtained only from the outermost surface layer and corresponds to around 1-μm thickness. It also depends on the selected analysis area, since fluctuations in composition may occur.

Figure 7 shows the temperature dependence of the tan δ and the storage modulus (E') for pure CA and HB/CA films. The maximum in the curve of the tan δ as a function of temperature is defined as the glass transition temperature (T_g) and the width of the glass transition can also be used as a criterion for the identification of structural heterogeneities in the materials. For pure CA [Fig. 7(a)], a tan δ peak at 173°C associated to T_g was observed and also no secondary relaxations in the range of temperature

TABLE II
Calculated and Experimental Atomic Silicon Content of HB/CA Nanocomposites

Sample	Calculated atomic silicon content (wt %) of the nanocomposites	Experimental atomic silicon content (wt %) at the nanocomposite free surface
HB/CA 10/90	0.90	1.82 ± 0.09
HB/CA 20/80	1.89	2.11 ± 0.10
HB/CA 30/70	2.67	3.04 ± 0.15

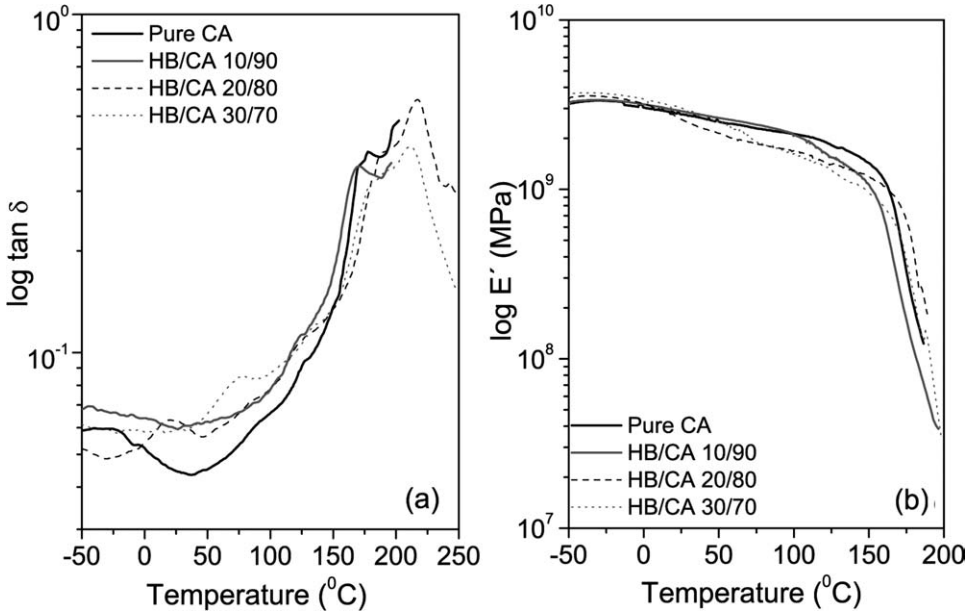

Figure 7 Dynamic-mechanical analysis for pure CA and HB/CA films: temperature dependence of (a) tan δ (b) storage modulus (E').

studied. The HB/CA (10/90) film presented a similar behavior to the pure CA film, with a T_g value of 170°C. On the other hand, secondary relaxations were observed in the range of ~ 20–195°C in the tan δ curves for the films with 20 and 30 wt % HB contents. This effect can be associated to the relaxation of the CA chain segments directly bonded to HB functional units. Moreover, T_g values for 20/80 and 30/70 HB/CA films were 218 and 212°C, respectively, and a shoulder at approximately 185°C was observed. As is known, an increase of the glass transition temperature is due to the restriction of the segmental motion of the polymer backbone and thus, in this study, could indicate the favorable interactions between the polymer and the siloxane domains observed by TEM. Considering that CA is a high-T_g polymer these increases, which were higher than 20%, are notable.

It was also observed that the maximum of the peak (T_g) of the HB/CA films became broader as the functional unit concentrations increased. This behavior is also associated with polymeric chain movement restrictions caused by the siloxane domains, which caused heterogeneities in the system, with different cross-linking densities.

The storage modulus (E') can be used to evaluate the reinforcement effect of the dispersed phase in the polymeric matrix, which is directly related to the interfacial strength between these materials. Figure 7(b) shows that, from −50 to 20°C, no significant differences in E' were obtained for the films, indicating that the siloxane nanodomains did not negatively interfere in the dynamical CA properties. Decreases of E' observed at 20 and 73°C for the HB/CA (20/80) and HB/CA (30/70) films, respectively, are due to secondary relaxations, as already discussed.

Therefore, the complex dynamic-mechanical behaviors of these films were a consequence of the heterogeneous morphologies of these materials.

CONCLUSIONS

The preparation of HB/CA nanocomposites, derived from CA and a multifunctional alkoxysilane precursor using the sol–gel process, is described. The rigidity of the films increased with the increase in the inorganic phase content. The thermal stability for the HB/CA films was similar to that shown by pure CA. The morphology of the materials was characterized by polysiloxane nanodomains dispersed in the cellulose matrix, which explains the observed complex dynamic-mechanical behavior. The HB/CA nanocomposites showed insolubility in organic solvents and reduction of the dimensional changes in water in comparison with CA.

References

1. Nguyen, T. P.; Lee, C. W.; Hassen, S.; Le, H. C. Solid State Sci 2009, 11, 1810.
2. Lin, C. H.; Chang, C. H.; Jao, W. C.; Yang, M. C. Polym Adv Technol 2009, 20, 672.
3. Wu, C.; Xu, T.; Gong, M.; Yang, W. J Membr Sci 2005, 247, 111.
4. Schottner, G. Chem Mater 2001, 13, 3422.
5. Pyun, J; Matyjaszewski, K. Chem Mater 2001, 13, 3436.
6. Wen, J; Wilkes, G. L. Chem Mater 1996, 8, 1667.
7. Schmidt, H. K.; Geiter, E.; Mennig, M.; Krug, H.; Becker, C.; Winkler, R.-P. J Sol-Gel Sci Technol 1998, 13, 397.

8. Chau, J. L. H.; Lin, Y.-M.; Li, A.-K.; Su, W.-F.; Chang, K.-S.; Hsu, S. L.-C.; Li, T.-L. Mater Lett 2007, 61, 2908.
9. Wang, X. Y.; Du, Y. M.; Luo, J. W. Carbohydr Polym 2007, 69, 41.
10. Park, H. M.; Mohanty, A. K.; Drzal, L. T.; Lee, E.; Mielewski, D. F.; Misra, M. J Polym Environ 2006, 14, 27.
11. Kim, J; Yun, S. Macromolecules 2006, 39, 4202.
12. Balser, K.; Eicher, T.; Wnadel, M.; Astheinmer, H. J. In Cellulose Esters. Ulmann's Encyclopedia of Industrial Chemistry; Gerhartz, W.; Yamamoto, Y. S., Eds.; VCH: New York, 1986, Vol. A5, p438.
13. Edgar, K. J; Buchanan, C. M.; Debenham, J. S.; Rundquist, P. A.; Seiler, B. D.; Shelton, M. C.; Tindall, D. Prog Polym Sci 2001, 26, 1605.
14. Zoppi, R. A.; Gonçalves, M. do C. J Appl Polym Sci 2002, 84, 2196.
15. Shojaie, S. S.; Rials, T. G.; Kelley, S. S. J Appl Polym Sci 1995, 58, 1263.
16. Mackenzie, J. D.; Bescher, E. J Sol-Gel Sci Technol 2003, 27, 7.
17. Mark, J. E.; Lee, C.; Bianconi, P. A.; Hybrid Organic-Inorganic Composites. Vol. 585; ACS: Washington, 1995.
18. Bandyopadhyay, A.; Bhowmick, A. R.; De Sarkar, M. J Appl Polym Sci 2004, 93, 2579.
19. Amerio, E.; Sangermano, M.; Malucelli, G.; Priola, A.; Voit, B. Polymer 2005, 46, 11241.
20. Hench, L. L.; West, J. K. Chem Rev 1990, 90, 33.
21. Brinker, C. J; Scherer, G. W. Sol-Gel Science: The Physics and Chemistry of Sol-Gel Processing; Academic Press: San Diego, 1990.
22. Avnir, D.; Braun, S.; Lev, O.; Ottolenghi, M. Chem Mater 1994, 6, 1605.
23. Keeling-Tucker, T.; Brennan, J. D. Chem Mater 2001, 13, 3331.
24. Nie, L.; Narayan, R. J Appl Polym Sci 1994, 54, 601.
25. Chen, W.; Su, Y.; Zhang, L.; Shi, Q.; Peng, J.; Jiang, Z. J Membr Sci 2010, 348, 75.
26. José, N. M.; Prado, L. A. S. A.; Yoshida, I. V. P. J Polym Sci Part B: Polym Phys 2004, 42, 4281.
27. Bellamy, L. J. The Infrared Spectra of Complex Molecules; John Wiley & Sons: New York, 1966.
28. Yuan, W.; Van Ooji, W. J. J Colloid Interface Sci 1997, 185, 197.
29. Toynbee, J Polymer, 1994, 35, 438.
30. Chatterjee, P. K.; Conrad, C. M. J Polym Sci Part A-1 Polym Chem 1968, 6, 3217.
31. Wu, S. In Polymer Handbook; Immergut E. H., Ed.; John Wiley & Sons: New York, 1989.